Journal of Materials Chemistry C

Accepted Manuscript

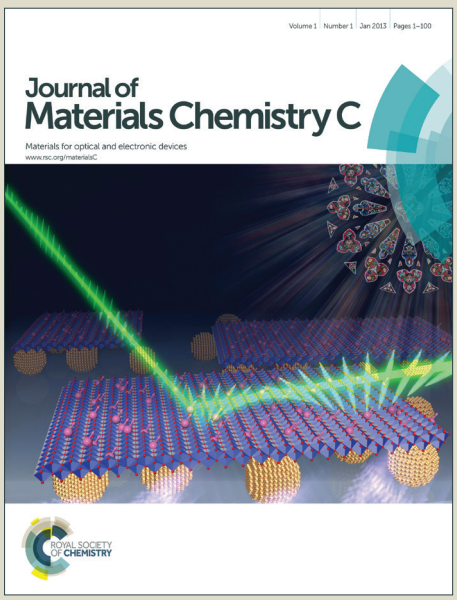

ROYAL SOCIETY OF CHEMISTRY

www.rsc.org/materialsC

Table of contents entry

Color graphic:

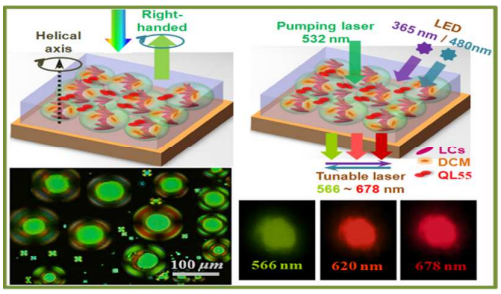

Text:

Light tunable lasing in photoresponsive chiral liquid crystal emulsion

Journal of Materials Chemistry C

Cite this: DOI: 10.1039/c0xx00000x

PAPER

www.rsc.org/xxxxxx

Wide tunable lasing in photoresponsive chiral liquid crystal emulsion †

Zhi-gang Zheng [a, b] *, Bo-wei Liu [a], Lu Zhou [a], Wei Wang [a], Wei Hu [b], Dong Shen [a]*

Received (in XXX, XXX) Xth XXXXXXXXX 20XX, Accepted Xth* XXXXXXXXX *20XX
DOI: 10.1039/c0xx00000x

A new tunable laser based on the photoresponsive chiral liquid crystal emulsion is reported. Such laser can be reversibly photo-tuned in a wide spectral range of 112 nanometers, and simultaneously possesses stable emission performances and quasi-continuous tunability. Typically, distinct from the conventional liquid crystal laser, such laser can be fabricated simply just by coating the material on the single substrate, which will simplify the production processes and broaden the application of liquid crystal laser. In addition, the mechanisms of the tunability are explored from the molecular scale. The studies reveal that the molecular conformation transition of photosensitive chiral switch during isomerization leads to the changes not only on the molecular geometry and the direction of dipole moment, but also on the molecular interactions and the miscibility of the materials. These changes cause the rearrangement of liquid crystals, thereby rendering the variation of helical twisted power and achieving the tuning on the photonic band edge of chiral liquid crystal, consequently forming the photo-tunable laser.

Introduction

Liquid crystals (LCs) are a kind of organic material with significant self-assembly. Due to the strong Van der Waals interaction between the molecules, LCs can form some ordered arrangements, such as the common nematic and smectic phases, without the aid of any external stimulus. By introducing the chiral center in the molecules or doping some chiral agents into LCs, the molecules are twisted and self-assembled into the helical structure, forming the chiral liquid crystals (CLCs). Such CLCs have the specific selective reflection characteristic for the circular polarized light with the same rotation sense with the CLCs as the wavelength is of the order of the helical pitch. Therefore the photons that match well with the CLC helix will be forbidden to propagate through the medium, which is called the effect of photonic band gap (PBG). The group velocity of photons in the vicinity of the band-edge is the minimum, thus the photon density of state (DOS) reaches the maximum correspondingly. If some fluorescent dyes are doped into the CLCs, and provided that the emission spectrum of the dye overlaps the band-edge of PBG, the lasing will be found at the edge under some certain pumping conditions, that is the so called band-edge CLC laser, which is promising to be used in the next generation laser displays or directly embedded onto the silicon to fabricate the lab-on-chip devices.[1]

The phenomenon of lasing in CLCs was firstly observed by Kopp *et al*.[2] After then, the theoretical work of Schmidtke *et al*. analyzed the lasing characteristics and discussed their correlations with the helical structure of CLCs.[3] In order to decrease the emission threshold as well as increase the lasing efficiency, a great deal of efforts had been made from the viewpoints of materials, *e.g.*, some kinds of polymer laser dyes and the dyes with extremely high quantum efficiency were synthesized,[4, 5] in addition, the LCs with higher anisotropic, better orderliness and larger elasticity were adopted.[6] Meanwhile the glass substrates of the LC cell were replaced by the high reflection silicon wafer[7] or the polymer CLCs layer[8, 9] to increase the optical gain length, and consequently decrease the emission threshold. The pumping conditions, including the incident angle,[10] the polarization[11] as well as the temperature,[12] were also optimized in theoretical and experimental.

One of excellent property of LCs is the response under the stimulus of external fields, such as the mechanical force, temperature, electric field and light, which makes the tunability of LC laser possible. In general, the large wavelength tuning range and the fast response are preferred for the LC laser. The largest wavelength shifting for about 80 nanometers by biaxially stretching CLC elastomer had been achieved.[13] As one of the most convenient tuning manner, electrically tunability of the emission intensity and wavelength have been widely studied, *e.g.*, the switching on and off of the lasing in polymer stabilized CLCs with less than 10 V had been reported in the recent;[14] the wavelength-shifting of the laser, normally less than 40 nanometers, had also been achieved in the defect mode device,[15] or the devices filled with some special LCs,[16, 17] or even the CLCs embedded nanopore network.[18] Light tuning manner always attracts widespread attentions as the advantages of easy and remote on demand controlling, independence on electrodes, and

high accuracy, comparing to the electric-field tuning. The wide wavelength tuning, realized from the photo-Fries rearrangement of chiral agent S811 or the photolysis of some certain chirals, were reported in the earlier time, however, the shortage is irreversibility of such tuning.[19, 20] Azo derivatives has the special reversible photoisomerization characteristic, which had been widely adopted in the light responsive materials and devices.[21-23] The nematic Azo- and Azoxy- components were mixed with the conventional photo-insensitive chiral dopant to form a photosensitive helical superstructure, resulting in a 70-nm-shifting of the laser.[24] Doping a small amount of Azo material in the CLCs can resolve such problem,[25] and a wider wavelength tuning range of 104 nanometers based on rod-like Azo chiral was fulfilled thanks to the work of Lin *et al*,[26] nevertheless, the response time for the tuning is long, generally takes a few or tens of minutes. By combining the photoisomerous Azo dyes and the high exitation efficiency quantum dots, the photo-tunable lasing with approximately 40 nm spectral shifting were realized as well.[27] Besides, the special tunable laser was proposed by introducing the helical pitch gradient in the cell, and the tunable lasing from 577 to 670 nm had been obtained.[28] The three layer structure, containing two CLC cell sandwiching a isotropic photoluminesence dye, with a wide tuning range was repported in recent.[29] Temperature is often considered as another convenient tuning manner. The tunable mode competition of the LC laser by means of temperature was reported a few months ago, indicating the prospect for the CLC laser to be used in the display.[30] For widening the wavelength tunable range in further, more than three kinds of laser dyes were doped in CLCs. By combining the effect of Förster energy transfer between the dyes with the spatial gradient of helical pitch, an ultra-wide tuning covered the whole visible spectrum band was achieved. However such system is not stable because of the diffusion between the dyes and the differences on the solubility thereof; in addition, the interaction of the transition moment between the dyes will decrease their quantum efficiency, leading to the weakening or even the disappearance of the lasing.[31-34]

Based on the mechanism of the band-edge lasing of CLCs, some new types of three-dimensional (3D) CLC lasers were developed, such as the lasing in the cubic blue phase liquid crystals (BPLCs),[35, 36] and in the spherical CLC droplets dispersions which can be tuned through the temperature as well as other external fields.[37, 38] Recently, Chen *et al*. reported a photo-tunable 3D laser formed by the Azo chiral doped CLC microshell, whereas, only about 50 nanometers wavelength-shifting was found.[39] In addition, the lasing induced by whispering-gallery-modes (WGM) resonances inside the LCs microstructures [40, 41] and the lasing pumped by two coherent beams [42] were found in the recent as well.

Due to the fluidity of LCs and the dispersions thereof, such materials should be sandwiched between two substrates in the real practice, and furthermore, the pre-treatments of the substrates are necessary and complex, therefore, restricting the miniaturization and simplification for the LC laser devices. Gardiner *et al*. prepared an emulsion by mixing the CLCs with the aqueous solution of poly-vinyl alcohol (PVA), and then coated the syrup on a planar glass to form a wet-film with randomly dispersed CLC droplets.[43] Different from the traditional random laser in polymer dispersed liquid crystal (PDLC) due to the feedback loops formed by the dispersed tiny LCs scatterers,[44] such wet-film shrunk in thickness in virtue of the deswelling, leading to the geometrical deformation of the dispersed LC droplets from sphere to oblate sphere with the diameter of tens of micrometers or larger, and meanwhile forcing the random aligned helical axis within the droplet changes to a uniform alignment vertical to the substrate. Consequently, the PBG effect, which is the requirement for the laser emission, was observed in the single substrate sample, similar as that of CLCs confined in pre-aligned cells. The CLC emulsion is independent of the LC cells, therefore, indeed simplifies the process for fabricating the LCs laser. However, with regard to the tunability of such single-substrate LC laser, there has been no report on this topic at present, which is the motivation of the studies herein.

Until now, a great many of studies on the tunable LC laser have been reported as mentioned above, while the first problem that the CLC emulsion laser faced to is which tuning manner is the most appropriate. Using the mechanical force or ambient temperature as the stimuli is inapposite, on account of the complex, large and heavy accessories. The electrically tunable seems more convenient than the above two, however two electrodes are necessary, thereby limiting such manner to be adopted in the CLC emulsion laser with only one or without electrode coated on the single substrate. The tunability in virtue of the spatial helical pitch gradient is also restricted for the reason that such arrangement of LCs is very difficult in the single substrate without enough anchoring. So, colligate the above, the photo-tuning is the only and most convenient way to realize the tunability of CLC emulsion laser. Secondly, for the reason that CLCs are normally photo-irresponsive, so the most common way to resolve the problem is doping a certain amount of photoisomerous guest materials into the CLCs host. Azo dyes are generally preferred because of its better photosensitivity, fast *trans*-to-*cis* transition, and good solubility with CLCs. Although the studies of photo-tunable CLC PBG by doping the azobenzene derivatives have been reported, the tuning performance was not satisfied. Li *et al*. proposed another Azo based binaphthyl derivatives with higher and photo-tunable chirality, which is referred to as light-driven chiral switch.[45-49] A series reports concerning the photo-tunability of CLCs doped with this kind of chiral switch have indicated an excellent photo-tunability performance, showing a rather wide shifting of PBG from the ultraviolet, spans the whole visible band, to the near infrared.[47, 48, 50] Thirdly, the wide emission band of laser dyes is another key point for obtaining the wide tunable lasing. As aforementioned, Förster energy transfer in multi-dyes-doped system seems effective for the wide tunable lasing, whereas accompanied by many problems which are contrarily harmful for the performances of the laser. Therefore, in view of these aspects, doping with the single laser dyes with wide emission band and good solubility in CLCs are the most preferable.

This paper reported a wide photo-tunable lasing in CLC emulsified film coated on the single substrate. The photo-tunability was obtained by mixing a small amount of Azo based binaphthyl chiral molecular switch within the CLC emulsion, which makes the emulsion possesses high photosensitivity, thereby realizing the wide shifting of PBG, and consequently

achieving the wide photo-tunability of the band-edge laser. To the best of our knowledge, such wide tunable emulsion laser by utilizing photosensitive chiral switch has not been reported previously. Moreover, the previous studies on tunable CLC laser mainly focus on the tuning performances, however little on the tuning mechanism. In this paper, the mechanism of the photo-tuning and their relevant influences on lasing performances were also investigated through the molecular simulations. The results coincide well with the experiments.

Experiments and molecular simulation methods

Sample preparations and testing

The conventional nematic LCs XH07-X (supported by Xianhua Chemical Co. Ltd., China) and the commercial chiral agent R811 (supplied from Merck, Germany) were mixed for preparing the CLCs. Simultaneously, some amount of photosensitive Azo based binaphthyl chiral switch (Fig. 1), with the same helical sense with R811, denoted as QL55, were doped into the CLCs, forming the photoresponsive CLCs system with the significant characteristic of photo-tunable PBG. The synthetic route of QL55 as well as the 1H NMR (400 MHz) spectra and the high resolution mass spectra used to identify the chemical structure of QL55 were given in Supplementary Information. The optimized contents for R811 and photosensitive chiral switch QL55 are 19.5 wt% and 2.5 wt%, respectively, and besides, 0.5 wt% of 4-(dicyanomethylene)-2-methyl-6-(4-dimethylaminostryl)-4H-pyan (DCM, supplied from Sigma-Aldrich) were doped as the laser dye. The helical twisted power (HTP) for the system can be tested through the common method of Grandjean-Cano wedge (supplied by Instec Co., Ltd.). Such mixture was blended with the aqueous solution of polyvinyl alcohol (PVA, supplied from Sigma-Aldrich) to obtain the emulsion with uniform CLC droplets dispersion. Subsequently, coating the emulsion onto a clean glass, forming the CLC emulsion wet film, and obtaining the dry film after the deswelling in consequence (Fig. S1). The size of the CLC droplets dispersed in the matrix of the dry film was 40~50 μm estimated through the scale bar fixed in the microscope, as shown in Fig. 2(a).

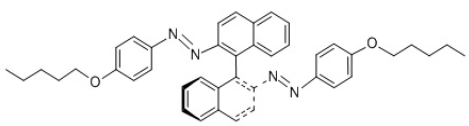

Fig. 1 Chemical structure of QL55.

The sample was excited by a second-harmonic Q-switched Nd: YAG pulsed laser (supplied by Beamtech Co., Ltd., Canada) with the output wavelength of 532 nm. The emission characteristics were detected by an optical fiber connected spectrometer (Avaspec-2048 from Avantes, Netherland), and the photo-tunability was conducted by the irradiation of LEDs with narrow spectral line width of 10 nm (Fig. S2).

Molecular simulation methods

The complete atomistic model was adopted for more accurate and comprehensive analyses of the molecular characteristics. The optimization of molecular geometry was carried out through the semi-empirical molecular orbit algorithm, AM1, which is an ideal choice when making tradeoff between the short calculation time and the accuracy, and has been proved to be effective and suitable to organic molecules.[51, 52] Both of the optimized geometrical configuration and the molecular dipole moment can be obtained in the calculation. Subsequently, some amounts of molecules were settled into a cubic box, and molecular dynamic (MD) methods were conducted under the restraint of periodic boundary conditions to simulate the macroscopic real material system. After the entire system reached thermal equilibrium, the characteristics of the materials, such as the molecular interaction energy, the solubility, the director and order parameter of LCs, at different situations were calculated. Some details of MD simulations, settings, and the calculation methods were presented in Supplementary Information.

Results and discussions

Characteristics of photosensitive CLC emulsion film

The emulsion containing with QL55 was coated on a glass substrate and observed through the microscope with reflection mode. As shown in Fig. 2(a), many green spherical zones randomly distribute throughout the view field. The green color is caused by the selective Bragg reflection of the CLCs with standing helix; while the blurry halation around the green zone is resulted from the anchoring of PVA interface which influences the original arrangement of LCs. Due to the reversible photoisomerization of QL55, the reflective color of the CLC droplets red-shifted during the irradiation of 365-nm-LED, and recovered after exposing with 480-nm-LED. When the photoisomerization reached thermal equilibrium, the color shifting stopped, thus the sample got to the photo-stationary state (PSS). And herein the PSS obtained through the UV (365 nm) and visible (480 nm) light irradiation is denoted by PSS_{UV} and PSS_{VIS}, respectively. In addition, it can be estimated from the scale bar that the size distribution of LC droplets is 30~100 μm, which approximately satisfies the normal distribution, with the statistical average of 72.4 μm. It should be noted that the droplet size is not only the size of the central Bragg reflection parts, but also including the size of the halation parts around the center. Figure 2(b) shows the PSS_{UV} of the droplet encircled in the white dash frame, after exposing by 365-nm-LED for 1 minute with the intensity of 9.2 mW/cm^2. The reflection color changes from the original green to red, due to the *trans*-to-*cis* photoisomerization of chiral switch, QL55. On the contrary, the recovery of reflection color can be realized though thermo-dynamic process within a relative long time or promoted by the irradiation with blue-green visible light. Figure 2(c) shows the PSS_{VIS} as the same droplet was exposed by 480-nm-LED with the intensity of 7.3 mW/cm^2 for 1 minute. It is easy to be found that the reflection color comes back to the original green, as similar as that in the initial state. The spectrums of the sample in two PSS states, shown in Fig. 2(d), present the evident reflection stop bands with the long wavelength band-edge (LWBE) at 566 nm and 680 nm corresponding to PSS_{VIS} and PSS_{UV}, respectively, thereby indicating that a good tunability of the band-edge within the range from 566 nm to 680 nm by light, which is crucial for the performance of the tunable laser. The HTPs of QL55 at the initial

state and two PSS states were tested and calculated as well (Eq. S1), which indicate a remarkable decrease from 49.0 μm^{-1}, for the initial state, to 17.1 μm^{-1}, for the PSS_{UV}; while an opposite increase from the PSS_{UV} to the PSS_{VIS} with the HTP of 40.1 μm^{-1}. As a result that the *cis*-QL55 can't completely transform into the *trans*-isomer within a short time after the exposure of visible light, HTP at PSS_{VIS} is a little smaller than that at the initial state. Such reason can also be interpreted by the differences of UV-Visible absorbance between PSS_{UV} and PSS_{VIS} (Fig. S3).

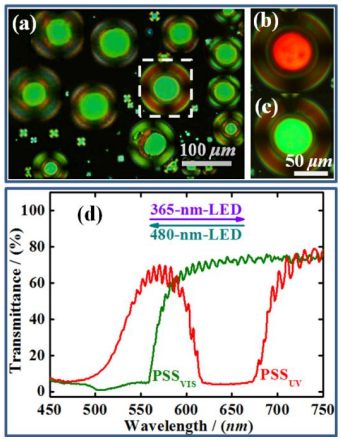

Fig. 2 Microscope photo of CLC emulsion film after the deswelling (a); the texture for the single CLC droplet in the white dashed box at PSS_{UV} (b) and PSS_{VIS} (c), and their corresponding transmittance spectrums (d).

Although the photo-tunable band-edge was achieved by doping QL55, some inner problems, such as why does the HTP change and how to change, are still not clear at present. To explore the hidden mechanisms, the molecular simulation was carried out. The optimized configurations for the two QL55 isomers were calculated firstly. Figure 3 shows the atomistic models of the *trans*-QL55 (the left-side) and the *cis*-QL55 (the right-side) isomers. Obviously, the two naphthalenes included in the QL55 molecule are not coplanar, but with a certain angle, regardless of *trans* or *cis* configurations. In addition, the calculation results reveal that the naphthalenes rotate with the axis of the σ bond, connecting two naphthalenes, during the photoisomerization. If defining the two naphthalenes with "A" and "B", as labeled in Fig. 3, when *trans*-to-*cis* transition occurs, A-unit rotates clockwise, while counter clockwise to B-unit (as labeled by the arrow with violet-color at the left side), forming the *cis*-isomer; however the opposite rotations (labeled by the cyan-color arrow at the right side) for the two units bring to the recovery from *cis*-isomer to the *trans* one. Therefore, the original helical arrangement of LCs is disturbed by such rotations under the effect of molecular cooperation, and then transforms to the other helical arrangement. Simultaneously, the direction of dipole moment of QL55 rotates as the isomerization, leading to the realignment of LC director due to the dipole interactions between LCs and QL55 molecules. As shown in the central inset of Fig. 3, the blue arrow is the direction of dipole moment at *trans*-configuration; while the green one corresponds to that at *cis*-configuration. One noteworthy result is that the direction of dipole moment left-handedly rotates during *trans*-to-*cis* isomerization, thereby rendering the LCs nearby rotate in the same manner to maintain the parallel of dipole moment between LCs and QL55 molecules. Such left-handed rotation causes the unwinding of the right-handed helical structure of LCs, thus the HTP of CLCs system is diminished gradually; however in the recovery process, similarly, the dipole moment rotate in opposite, causing the increasing of HTP. Such results show in agreement with that of experiments.

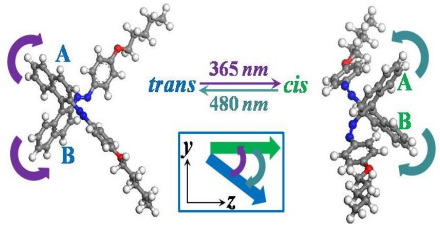

Fig. 3 Molecular conformation transformation of QL55 between the *trans* and *cis* isomers. The inset at the lower center depicts the rotation of the direction of the dipole moment; the blue arrow is the direction of the dipole moment for *trans*-QL55, while the green one is that for *cis*-QL55.

The LC arrangements influenced by *trans*-QL55 and *cis*-QL55 were calculated in accordance with the MD methods. As shown in Fig. 4(a), there is an evident twist of the LC director when the QL55 molecules are *trans*-isomer (left-side); whereas, such twist is significantly weakened in the case that *trans*-QL55 is replaced by *cis*-QL55. The extent of the twist can be evaluated by calculating the angle between the LC directors, near the top and bottom of the simulated box; while the LC director can be calculated through the statistical average for the direction of every LC molecular long axis (director of LC molecule). For the convenience of comparison, the directors are expressed as the vector containing azimuth angle (φ) and polar angle (θ). Figure 4(b) presents the LC directors near the bottom and top in Cartesian coordinate. The left-side of Fig. 4(b) corresponds to the case of *trans*-QL55/LC system, showing that LC directors near the bottom and top are $\mathbf{n}_{bottom}=(\varphi, \theta)=(45.0°, 89.5°)$ and $\mathbf{n}_{top}=(\varphi, \theta)=(84.9°, 89.3°)$, respectively. Note that the polar angle, θ, is almost unchanged in the helical arrangement, thus the twisted angle can be simply calculated by the difference of the azimuth angle, φ, which is 39.9°. In addition, it is found that LC director from the bottom to the top rotates clockwise, thereby proving that *trans*-QL55 presents the characteristic of R-chirality, which is consistent with the fact. Similarly, LC directors in the system containing *cis*-QL55, shown in the right-side of Fig. 4(b), are respectively $\mathbf{n}_{bottom}=(\varphi, \theta)=(61.0°, 89.5°)$ and $\mathbf{n}_{top}=(\varphi, \theta)=(70.9°, 89.6°)$. Similarly, the twisted angle is 9.9°, which indicates a weak twisted helix, however, invariability of the R-chirality. Another interesting aspect of the calculation is that the HTP of *trans*- or *cis*- QL55 can be estimated through the results obtained above. For instance, combining the twisted angle of *trans*-QL55/LC system, 39.9°, and the dimension of the corresponding cubic box, 80.52 Å, the helical pitch (P) can be calculated as 80.52×360°/39.9°=72.65 nm; while the mass percentage (C) of *trans*-QL55 can be calculated by the number of molecules in the cubic box (960 5CB LCs and 128 *trans*-QL55) and the molecular weight (249.36 g/mol for 5CB molecule and 634.82 g/mol for *trans*-QL55), thereby obtaining the mass percentage of *trans*-QL55 is (128×634.82)/(960×249.36+128×634.82)=25.34 wt%; therefore, the HTP of *trans*-QL55 is $1/(P \cdot C)=1/(72.65\times25.34$ wt%) $nm^{-1}=54.3$ μm^{-1}. With the same method, HTP of *cis*-QL55

Interactions (kcal/mol)	$E_{int}=E_{ele}+E_{vdw}$	$E_{ele}=\sum_{i>j}\frac{q_i q_j}{\varepsilon r_{ij}}$	$E_{vdw}=\sum_{i>j}\left[\frac{A_{ij}}{r_{ij}^9}-\frac{B_{ij}}{r_{ij}^6}\right]$
trans-QL55/LC	-385.98	-286.23	-99.75
cis-QL55/LC	-310.69	-235.13	-75.56
LC/LC	-273.08	-211.76	-61.23

is calculated as 1/(292.80×25.34 wt%) nm^{-1}=13.5 μm^{-1}. The estimated values are approximately consistent with the experimental results obtained through Grandjean-Cano wedge, *i.e.*, 49.0 μm^{-1} for *trans*-QL55 and 17.1 μm^{-1} for *cis*-QL55, with only a deviation of 10~20%. Such deviation comes from impurity of QL55 isomers in the system, that is to say the *trans*-QL55 may contain some small amounts of *cis*-QL55, and vise versa; while in the simulated model, QL55 isomer is completely pure.

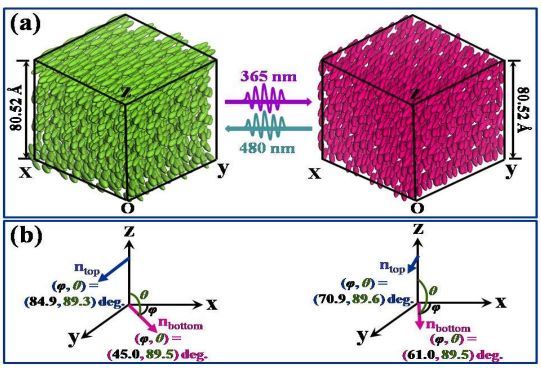

Fig. 4 LC arrangements as QL55 switch are *trans*-configuration and *cis*-configuration, respectively (a) and the direction of LC director denoted in Cartesian coordinate (b).

Subsequently, the interaction energy (E_{int}) between LCs and QL55 isomers were calculated (Eq. S2) to explore the interaction variations of the system brought by the configuration transformation due to the photoisomerization. Table 1 shows the interaction energies between QL55 isomers and the LCs; besides, the interaction energy between LC molecules is listed for comparison. The minus of the calculated results means that the blend systems of QL55 and LCs are stable, while the strength of the interaction is represented by the corresponding absolute value. It is evident that the interaction between the *trans*-QL55 and LCs is about 75 kcal/mol stronger than that between the *cis*-QL55 and LCs, which indicates the weakening of twisted power during the isomerization of QL55. It is also found that, comparing these interactions with LC molecular interaction, the energy between LCs is significantly weaker than that between LCs and QL55, no matter which configuration is. In general, the nematic alignment of LCs is maintained by the molecular interaction, while the stronger interactions between *trans*- (*cis*-) QL55 and LCs may lie in the contribution from helical twisted energy. The static electric energy part (E_{ele}) and Van der waals part (E_{vdw}) expressed by the 9-6 Lennard-Jones function[53, 54] were also listed respectively in the third and fourth rows of Table 1, and it can be noted that the major factor that causes the weakening of interaction energy in *trans*-to-*cis* isomerization is the decreasing of static electric energy part; while such decreasing is attributed to the lengthening of molecular spacing, since that the static electronic energy is inversely proportional to the molecular spacing.

Table 1. Molecular interaction energies calculated through MD.[a)]

[a)] q_i and q_j represent the electronic charge of molecule i and j, respectively; r_{ij} is the distance between the corresponding molecules; A_{ij} and B_{ij} are the Van der waals interaction parameters; $\sum$ denotes the summation of energy between the molecules contained in the system.

The total quantity of electronic charge for the system is constant during the isomerization, therefore, E_{ele} is only determined by the molecular spacing, r_{ij}.

Furthermore, from the viewpoint of molecular geometry, the Azo groups in *trans*-QL55 show the rod like configuration which is very similar with the conventional LC molecules, while the corresponding *cis*-isomer presents a distinct configuration of bent-shape, therefore it can be predicted that the miscibility between *trans*-QL55 and LCs is better. To prove it, the solubility parameters of two QL55 isomers were respectively calculated (Eq. S3) and then compared with the solubility of 5CB (the solubility of our LCs is considered to be similar with that of 5CB, because the major component of our LCs is 5CB, >60 mol%) reported in the previous publications.[54] As the results shown that the solubility parameter of *trans*-QL55 is 18.10 $(J\cdot cm^3)^{0.5}$, which is 3.8 $(J\cdot cm^3)^{0.5}$ higher than that of *cis*-QL55, whereas only 0.8 $(J\cdot cm^3)^{0.5}$ lower than that of 5CB, thereby indicating a significant better miscibility between *trans*-QL55 isomer and the LCs owing to their closer solubility parameters. The drop of the miscibility, when the rod like *trans* configuration transforms to the bent-shaped *cis* one, may influence the helical structure from two aspects. On the one hand, the higher solubility of *trans*-QL55 leads to a stronger twisted power of the CLCs, thereby shortening the helical pitch; contrarily, the lower solubility of *cis*-QL55 resulting in a lengthening of the pitch because of the weakening of twisted power. On the other hand, the good miscibility of *trans*-QL55/CLC system causes a better dispersion of *trans*-QL55 in CLCs, which decreases the molecular spacing and leads to the stronger molecular interactions, therefore, shortens the helical pitch.

Tunable lasing in CLC emulsion

As aforementioned, the helical axes of the CLC droplets randomly arrange in the wet-film, causing the light scattering, thereby leading to the disappearance of the PBG effect, consequently influencing the lasing performances of the film. However, after the deswelling of the wet-film, the standing helix forms in CLC droplet due to the shrinkage of such film, therefore establishes the fundamental structure of 1D PBG laser chamber. Such standing helix was confirmed firstly by observing the texture of CLC droplet and comparing the texture as the sample was rotated with the central vertical axis of the objective stage. As shown in Fig. 5(a), there are many concentric circles from the center to the edge of the droplet, and become more and more obscure because of the oblate spherical surface of the CLC droplets. Similarly, the halation around the edge caused by the interfacial anchoring is still visible. As the sample is rotated by 90° from the original position (0°), the texture before and after

the rotation are compared, whereas no differences is discerned, whether on the color, brightness or the profile, which indicates the standing helix is established in the CLC droplets. Moreover, the laser emission on the normal direction of the substrate, detected in the front and 50-mm away from the sample, further proves the formation of standing helix.

Subsequently, the lasing performance and the photo-tunability were tested. Figure 5(b) shows the spectrums of the laser versus the duration of irradiation by 365-nm-LED with the intensity of 9.2 mW/cm2. At the initiation, the laser emission with the wavelength of 566 nm, corresponding to the position at LWBE of PSSVIS, is found (spectrum I); as the continual irradiation, the emission wavelength red-shifts gradually, passing through 594 nm (spectrum II) for 2-second-exposure, 620 nm (spectrum III) for 7-second-exposure, 652 nm (spectrum IV) for 23-second-exposure, until reaches the position at 678 nm (spectrum V), which is very close to the LWBE of PSSUV, ~680 nm, after irradiation for 50 seconds. On the contrary, if the exposure source is replaced by 480-nm-LED, the wavelength of laser blue-shifts, starting from 678 nm and finally returning back to the original position at 566 nm within 55 seconds as the exposure intensity is 7.3 mW/cm2, therefore achieving the photo-tunable laser, which can be tuned back and forth in the wide range of 112 nanometers, from 566 nm to 678 nm. The emission intensity is determined by the quantum efficiency at the corresponding wavelength if the pumping energy is constant; in other words, the equal emission intensity for the laser with different wavelengths can be obtained by modulating the pumping energy. The laser emission thresholds (LETs) were tested as shown in Fig. 5(c). The LET of 566-nm-laser and 678-nm-laser are 1.05 μJ/pulse and 1.12 μJ/pulse, respectively. Such thresholds are very close to each other, with only less than 0.1-μJ/pulse higher, comparing LET of 678-nm-laser with that of 566-nm-laser; however, as the pumping energy exceeds the thresholds, a great difference on the slopes of the curves generates, showing the evidently higher slope of 566-nm-laser than that of 678-nm-laser. Such difference is considered to be attributed to the higher quantum efficiency of DCM at 566 nm. The line width (Δλ) of the laser is estimated to 1.4~1.5 nm, however, considering that the value is very close to the resolution limit of the spectrometer, 1.4 nm, therefore the real line width of the laser is supposed to be narrower. Figure 5(d) presents three CCD photos of laser spots, with the color of yellow-and-green, orange red and bright red, correspond to the wavelength of 566 nm, 620 nm, and 678 nm, respectively. The brightness profiles of the spots are very similar to Gaussian distribution, which coincide with the characteristic of the laser. However, the interference ring around the spot, usually found in the conventional CLC laser, is not found, due to the thickness of the dry-film, 50~60 μm, is much larger than other conventional CLC cell, 10 μm, which results in the weak interferences. It is noteworthy that such better lasing performance is closely dependent on the size of LC droplet, especially the size of central Bragg reflection part. The larger LC droplet is, the better lasing performances are, and consequently, the wider spectral shifting of the laser is. It was found that the emission intensity was weaker and weaker as the decreasing of the droplet size, and even disappeared as the droplet smaller than 20 μm. To obtain the large droplets dispersion, a lower stirring rate of 90 rmp (the details were given in the Supplementary Information) was maintained. Look back on Fig. 2(a), the film containing larger droplet size, with the central Bragg reflection parts of 40~50 μm, was used in the experiments.

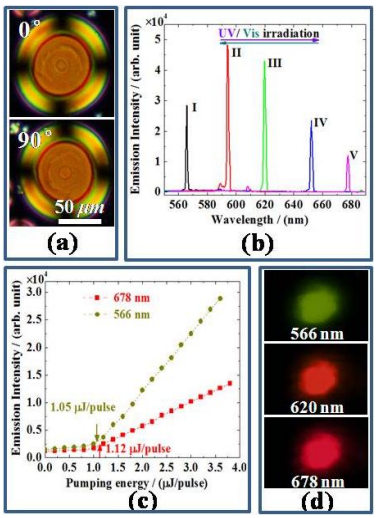

Fig. 5 Textures of CLC droplets observed with transmission mode (a); the spectrums of lasers during the photo-tuning (b); the relationships of pumping energy versus emission intensity of 566-nm-laser and 678-nm-laser (c); and the photos of laser spots at 566 nm, 620 nm, and 678 nm, respectively (d).

Note that the wavelength of pumping source is 532 nm, which is also contained into the absorption spectral range of Azo material, rendering the *cis*-to-*trans* isomerization of Azo group. That is to say the photosensitivity for CLC system doped with pure Azo-derivatives is very strong, which is not beneficial to the stability of the material under the ambient light. The previous publication reported that the laser emitting was generally accompanied by an evident wavelength-shifting in the pure Azo-dye doped CLC laser.[39] To confirm whether such shifting occurs in the CLC emulsion laser mentioned herein, the material was modulated to the PSS_{UV} firstly, and then followed by pumping the material with the energy about 3.0 μJ/pulse at the dark condition and simultaneously detecting the wavelength of the laser. However, what is exciting is that no obvious wavelength-shifting was found, even after the sample was pumped 20 times. Such good photo-stationary may be related with the low content of photosensitive Azo-derivative, QL55. Besides, the lower pumping energy is another factor, while such energy is determined by the LET, and increases with the rising of the LET; the higher LET directly leads to the higher pumping energy and thereby decreases the photo-stability of the sample. Therefore, it can be considered that the lower LET is one of requirement for obtaining an ideal photo-stationary CLC emulsion laser.

In addition, as Lin *et al*. reported, there appears another weak laser at the short wavelength band-edge (SWBE) as the pumping energy is about three times of the threshold.[26] The lasing position, either at LWBE or SWBE, is determined by the direction of transition moment of the laser dye molecule with respect to the direction of the LC director, in accordance with the prior theoretical work.[3] As the transition moment is parallel to the LC director, lasing at LWBE occurs; while as they are perpendicular with each other, lasing at SWBE appears. Considering that the laser dye used in Lin's and our experiments are the same, DCM; and many experimental results have been proved that the preferred orientation of transition moment for DCM is parallel to the LC director,[55] accordingly, the emission energy of LWBE lasing could be lower than that of SWBE lasing. Therefore, the

possible reason for the appearance of SWBE lasing may be related with the disordered alignment of LCs, occurring in the photoisomerization which distorts the original direction of transition moment, thereby causing the transition moment perpendicular to the LC director in some parts of the system, and consequently decreasing the laser emission threshold at SWBE which makes the SWBE laser is easier to be pumped out under a lower pumping energy. Whereas, not similar as the previous report, the SWBE lasing was not observed in the tunable lasing presented herein, as the pumping energy was controlled to 3.0 μJ/pulse (about three times of the threshold energy). , The strong interaction between the LCs and the QL55 isomers is considered to be a possible interpretation. Under such strong interaction, the distribution of LC director is constrained, thereby keeping an ordered alignment of LCs during the photo-tuning, therefore rising the threshold emission energy at SWBE. To make the analysis more understandable, the order parameter of LCs near the QL55 isomers were calculated. The helical alignment of LCs can be simply approximated as the well-aligned nematic LCs, because the effective interaction distance between QL55 and LCs is much smaller compared with the helical pitch of the CLCs; while in such small range, the helical structure can be ignored and replaced by a well-aligned nematic alignment. Under such approximation, the order parameters of LCs in the systems of *trans*-QL55/LC (LCs mixed with *trans*-QL55), *trans*+*cis*-QL55/LC (LCs mixed with *trans*- and *cis*- QL55) and *cis*-QL55/LC (LCs mixed with *cis*-QL55) were calculated as 0.60, 0.59 and 0.57, respectively, indicating that the influence of photoisomerization on the order of LC alignment is so weak that can be neglected. To explore this from the experimental viewpoint in further, the transmittance spectrums of the deswelling film were detected during the UV and visible light irradiations (Fig. S4), because that the arrangement of LCs can be reflected from the changes of the spectrum. Interestingly, although there is the evident shifting of the spectrums, the features of the spectrums, such as the shape, the transmittance at the stop band and the band width, are almost invariable during the photo-tuning, thereby it can be speculated that the well-defined helical structure was maintained, except for the variation of the pitch. The suppression of SWBE lasing is obviously an improvement for the smoothly application of such tunable laser.

The continuously tuning for the wavelength of laser is always concerned by the researchers, however it is hard to be achieved in the conventional CLCs encapsulated in the antiparallel proceeded planar cells.[56] The reason is that the strong anchoring on the inner surfaces of two substrates compels the LCs near the surfaces align in parallel, causing a discrete pitch-tuning following the relationship, in which the cell gap is equal to the integer times of the half of the pitch. Thus the continuity of photo-tuning for the deswelling film was explored by detecting the shifting of LWBE where the laser emission occurs, during the light irradiation. The light intensities for 365-nm-LED and 480-nm-LED sources are the same as the aforementioned, 9.2 mW/cm^2 and 7.3 mW/cm^2, respectively. Considering the fast shift of LWBE under the corresponding intensities, the time step for auto-saving a spectrum was set as 200 milliseconds. As shown in Fig. 6, basically, a better continuously photo-tuning is obtained, regardless of red-shifting triggered by 365-nm-LED, or the blue-shifting promoted by 480-nm-LED, only with some unobvious jumps of the LWBE within 10 to 30 seconds duration of irradiation, labeled by the dashed frames with the violet color and the cyan color, respectively. The extent of such jumps are very small, about 2~3 nm. Therefore, it can be considered that the photo-tuning of the CLC emulsion laser is quasi-continuous. Such quasi-continuity might be closely related with the weak anchoring of the substrate, owing that for one thing, there is only one substrate without the orientational process; for another, the thickness of the film is several times thicker than that of conventional CLC layer confined in the cell, which causes the weakening of the surface tension to the LCs, for the reason that the surface tension is inversely proportional to the distance between the LCs and the substrate. Such weak anchoring causes the aforementioned small jump of LWBE.

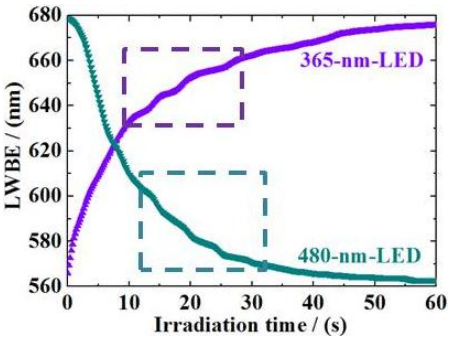

Fig. 6 LWBE versus the irradiation time. The jumps are denoted in the dashed frames.

Conclusions

The wide tunable laser in the photoresponsive CLC emulsion is demonstrated in this paper. The wavelength of the laser can be tuned reversibly in a wide spectral range, from 566 nm to 678 nm, by the irradiation with UV and visible light sources. The mechanisms for the photo-tunability, explored on the molecular viewpoints through the MD simulations, indicate that the molecular conformation of the photosensitive chiral switch QL55 changes reversibly due to the photoisomerization, and simultaneously causes the variation of molecular geometry and the rotation of the direction of dipole moment, thereby rendering the rearrangement of LCs compelled by the strong molecular interaction energy, and finally leads to the change of HTP under the long range interaction between LCs. In addition, the change of molecular structure simultaneously causes the different miscibility of QL55 isomers that blended into the LCs, *i.e.*, the *trans*-isomers have a better miscibility with LCs than that of the *cis*-isomers, which influences the molecular interactions and the HTP as well. Due to the strong interactions, the well-defined helical structure of CLCs is maintained during the photo-tuning, which ensures the stable laser emission at LWBE. The quasi-continually tuning is achieved as well because of the weak surface anchoring in the system. Such study provides a new material with wide photo-tunable and well-performed laser emission based on photoresponsive CLC emulsion, and typically, molecular simulations are adopted for well understand the mechanisms of the photo-tuning. The results also reveal that such wide photo-tunable laser can be fabricated simply just by coating

the material onto the single substrate, which will be promising in the future photonic devices or the low-cost laser displays.

Acknowledgements

This work is sponsored by the National Science Foundation of China (grant No. 61435008, No. 61108065), the Chen-guang Talent Foundation of Shanghai Education and Development Committee (grant No. 12CG32), and the Foundation of Laboratory of Solid State Microstructures, Nanjing University (grant No. M27005).

Notes and references

[a]*Department of Physics, East China University of Science and Technology, No.130, Meilong Road, Shanghai, 200237, China. E-mail: zgzheng@ecust.edu.cn, shen@ecust.edu.cn; Tel.: +86-21-64253514; Fax: +86-21-64253514.*

[b]*National Laboratory of Solid State Microstructures and College of Engineering and Applied Sciences, Nanjing University, Nanjing 210093, China*

† Electronic Supplementary Information (ESI) available: [details of any supplementary information available should be included here]. See

DOI: 10.1039/c0xx00000x/

1 H. Coles, S. Morris, *Nat. Photonics*, 2010, **4**, 676.
2 V. I. Kopp, B. Fan, H. K. M. Vithana, A. Z. Genack, *Opt. Lett.*, 1998, **23**, 1707.
3 J. Schmidtke, W. Stille, *Eur. Phys. J. B*, 2003, **31**, 179.
4 F. Araoka, K. Shin, Y. Takanishi, K. Ishikawa, H. Takezoe, Z. Zhu, T. M. Swager, *J. Appl. Phys.*, 2003, **94**, 279.
5 M. Uchimura, Y. Watanabe, F. Araoka, J. Watanabe, H. Takezo, G. Konishi, *Adv. Mater.*, 2010, **22**, 4473.
6 S. M. Morris, A. D. Ford, M. N. Pivnenko, O. Hadeler, H. J. Coles, *Phys. Rev. E*, 2006, **74**, 061709.
7 C. Mowatt, S. M. Morris, T. D. Wilkinson, H. J. Coles, *Appl. Phys. Lett.*, 2010, **97**, 251109.
8 K. Amemiya, M. H. Song, Y. Takanishi, K. Ishikawa, S. Nishimura, T. Toyooka, H. Takezoe, *Jpn. J. Appl. Phys.*, 2005, **44**, 7966.
9 Y. Zhou, Y. Huang, S. T. Wu, *Opt. Express*, 2006, **14**, 3906.
10 L. Penninck, J. Beeckman, P. De Visschere, K. Neyts, *Phys. Rev. E*, 2012, **85**, 041702.
11 Y. Matsuhisa, Y. Huang, Y. Zhou, S. T. Wu, R. Ozaki, *Appl. Phys. Lett.*, 2007, **90**, 091114.
12 S. M. Morris, A. D. Ford, M. N. Pivnenko, H. J. Coles, *J. Appl. Phys.*, 2005, **97**, 023103.
13 H. Finkelmann, S. T. Kim, A. Munoz, P. Palffy-Muhoray, B. Taheri, *Adv. Mater.*, 2001, **13**, 1069.
14 B. Liu, Z. Zheng, X. Chen, D. Shen, *Opt. Mater. Express*, 2013, **3**, 519.
15 M. H. Song, B. Park, K. C. Shin, T. Ohta, Y. Tsunoda, H. Hoshi, Y. Takanishi, K. Ishikawa, J. Watanabe, S. Nishimura, T. Toyooka, Z, Zhu, T. M. Swager, H. Takezoe, *Adv. Mater.*, 2004, **16**, 779.
16 T. H. Lin, H. C. Jau, C. H. Chen, Y. J. Chen, T. H. Wei, C. W. Chen, Andy Y. G. Fuh, *Appl. Phys. Lett.*, 2006, **88**, 061122.
17 M. Kasano, M. Ozaki, K. Yoshino, D. Ganzke, W. Haase, *Appl. Phys. Lett.*, 2003, **82**, 4026.
18 Y. Inoue, H. Yoshida, K. Inoue, Y. Shiozaki, H. Kubo, A. Fujii, M. Ozaki, *Adv. Mater.*, 2011, **23**, 5498.
19 A. Chanishvili, G. Chilaya, G. Petriashvili, R. Barberi, R. Bartolino, G. Cipparrone, A. Mazzulla, L. Oriol, *Adv. Mater.*, 2004, **16**, 791.
20 S. Furumi, S. Yokoyama, A. Otomo, S. Mashiko, *Appl. Phys. Lett.*, 2004, **84**, 2491.
21 H. Yu, T. Ikeda, *Adv. Mater.*, 2011, **23**, 2149.
22 H. Yu, C. Dong, W. Zhou, T. Kobayashi, H. Yang, *Small*, 2011, **7**, 3039.
23 L. Yu, Z. Cheng, Z. Dong, Y. Zhang, H. Yu, *J. Mater. Chem. C*, 2014, **2**, 8501.
24 G. Chilaya, A. Chanishvili, G. Petriashvili, R. Barberi, R. Bartolino, G. Cipparrone, A. Mazzulla, P. V. Shibaev, *Adv. Mater.*, 2007, **19**, 565.
25 Andy Y. G. Fuh, T. H. Lin, J. H. Liu, F. C. Wu, *Opt. Express*, 2004, **12**, 1857.
26 T. H. Lin, Y. J. Chen, C. H. Wu, Andy Y. G. Fuh, J. H. Liu, P. C. Yang, *Appl. Phys. Lett.*, 2005, **86**, 161120.
27 L. J. Chen, J. D. Lin, C. R. Lee, *J. Mater. Chem. C,* 2014, **2**, 4388.
28 Y. Huang, Y. Zhou, S. T. Wu, *Appl. Phys. Lett.*, 2006, **88**, 011107.
29 G. Petriashvili, M. A. Matranga, M. P. De Santo, G. Chilaya, R. Barberi, *Opt. Express*, 2009, **17**, 4553.
30 J. H. Lin, P. Y. Chen, J. J. Wu, *Opt. Express*, 2014, **22**, 9932.
31 A. Chanishvili, G. Chilaya, G. Petriashvili, R. Barberi, R. Bartolino, G. Cipparrone, A. Mazzulla, R. Gimenez, L. Oriol, M. Pinol, *Appl. Phys. Lett.*, 2005, **86**, 051107.
32 K. Sonoyama, Y. Takanishi, K. Ishikawa, H. Takezoe, *Jpn. J. Appl. Phys.*, 2007, **46**, L874.
33 P. J. W. Hands, C. A. Dobson, S. M. Morris, M. M. Qasim, D. J. Gardiner, T. D. Wilkinson, H. J. Coles, *Proc. SPIE*, 2011, 8114-28.
34 A. Chanishvili, G. Chilaya, G. Petriashvili, R. Barberi, R. Bartolino, G. Cipparrone, A. Mazzulla, R. Gimenez, L. Oriol, M. Pinol, *Appl. Phys. Lett.*, 2005, **86**, 051107.
35 W. Cao, A. Munoz, P. Palffy-Muhoray, B. Taheri, *Nat. Mater.*, 2002, **1**, 111.
36 S. T. Hur, B. R. Lee, M. J. Gim, K. W. Park, M. H. Song, S. W. Choi, *Adv. Mater.*, 2013, **25**, 3002.
37 M. Humar, I. Musevic, *Opt. Express*, 2010, **18**, 26995.
38 J. D. Lin, M. H. Hsieh, G. J. Wei, T. S. Mo, S. Y. Huang, C. R. Lee, *Opt. Express*, 2013, **21**, 15765.
39 L. Chen, Y. Li, J. Fan, H. K. Bisoyi, D. A. Weitz, Q. Li, *Adv. Opt. Mater.*, 2014, **2**, 845.
40 M. Humar, M. Ravnik, S. Pajk, I. Musevic, *Nat. Photonics*, 2009, **3**, 595.
41 K. Peddireddy, V. S. R. Jampani, S. Thutupalli, S. Herminghaus, C. Bahr, I. Musevic, *Opt. Express*, 2013, **21**, 30233.
42 Z. V. Wardosanidze, A. Chanishvili, G. Petriashvili, G. Chilaya, *Opt. Lett.*, 2014, **39**, 1008.
43 D. J. Gardiner, S. M. Morris, P. J. W. Hands, C. Mowatt, R. Rutledge, T. D. Wilkinson, H. J. Coles, *Opt. Express*, 2011, **19**, 2432.
44 S. Gottardo, S. Cavalieri, O. Yaroshchuk, D. S. Wiersma, *Phys. Rev. Lett.*, 2004, **93**, 263901.
45 Y. Wang, Q. Li, *Adv. Mater.*, 2012, **24**, 1926.
46 Q. Li, Y. Li, J. Ma, D. K. Yang, T. J. White, T. J. Bunning,

Adv. Mater., 2011, **23**, 5069.
47 T. H. Lin, Y. Li, C. T. Wang, H. C. Jau, C. W. Chen, C. C. Li, H. K. Bisoyi, T. J. Bunning, Q. Li, *Adv. Mater.*, 2013, **25**, 5050.
48 T. J. White, R. L. Bricker, L. V. Natarajan, N. V. Tabiryan, L. Green, Q. Li, T. J. Bunning, *Adv. Funct. Mater.*, 2009, **19**, 3484.
49 H. K. Bisoyi, Q. Li, *Acc. Chem. Res.*, 2014, **47**, 3184.
50 J. P. Vernon, A. D. Zhao, R. Vergara, H. Song, V. P. Tondiglia, T. J. White, N. V. Tabiryan, T. J. Bunning, *Opt. Express*, 2013, **21**, 1645.
51 D. L. Cheung, S. J. Clark, M. R. Wilson, *Chem. Phys. Lett.*, 2002, **365**, 140.
52 Z. Zheng, D. Shen, P. Huang, *New J. Phys.*, 2010, **12**, 113018.
53 M. J. Hwang, T. P. Stockfisch, A. T. Hagler, *J. Am. Chem. Soc.*, 1994, **116**, 2515.
54 Z. Zheng, J. Ma, Y. G. Liu, L. Xuan, *J. Phys. D: Appl. Phys.*, **41**, 235302.
55 A. D. Ford, S. M. Morris, M. N. Pivnenko, C. Gillespie, H. J. Coles, *Phys. Rev. E*, 2007, **76**, 051703.
56 K. Funamoto, M. Ozaki, K. Yoshino, *Jpn. J. Appl. Phys.*, 2003, **42**, L1523